SIMULATION OF THE WATER CYCLE INCLUDING HDO/H2O ISOTOPIC FRACTIONATION ON THE PRESENT MARS USING DRAMATIC MGCM

T. Kuroda, *National Institute of Information and Communications Technology, Koganei, Tokyo, Japan (tkuroda@nict.go.jp).*

Introduction:

The spacecraft on the Mars orbit, such as Mars Global Surveyor (MGS), Mars Odyssey, Mars Express and Mars Reconnaissance Orbiter (MRO), have continuously observed the global distributions of water vapor and water ice clouds for these 17 years. Simulating the water cycle on Mars consistently with those observations using Martian General Circulation Models (MGCMs) is a challenging topic, as the required physical processes are not well known.

First simulations of the Martian water cycle which incorporated the observations were made by Richardson and Wilson [2002] and Richardson et al. [2002], assuming the prescribed ice cloud radius of 2 μm to determine the sedimentation velocity. Montmessin et al. [2004] first introduced the cloud microphysics which was substantially important for the reproduction of the realistic seasonal and latitudinal variances of the water ice opacity. In those studies the radiative effects of water ice clouds were missing, but later Wilson et al. [2008] first showed the importance of them on the temperature fields. The development of a model which consistently reproduces the water cycle with radiatively-active water ice clouds has been difficult [e.g. Haberle et al., 2011], although Navarro et al. [2014] indicated that the scavenging of dust particles due to the condensation ice also plays a significant role.

In this context, we are also simulating the water cycle of the present Martian environment using the DRAMATIC (Dynamics, RAdiation, MAterial Transport and their mutual InteraCtions) MGCM [Kuroda et al., 2005, 2013, 2015] whose dynamical core is based on the CCSR/NIES/ FRCGC MIROC model [K-1 Model Developers, 2004] for the further investigations of the water cycle system and related material transport on Mars. A lot of improvements to fit the observed features have been made since the earlier efforts shown in Kuroda et al. [2008, 2012]. Also the HDO/H_2O isotopic fractionation process have been implemented into the DRAMATIC MGCM, and the simulated results of HDO/H_2O ratio distributions are also shown.

Model Description:

The MGCM has a spectral solver for the three-dimensional primitive equations. The basic runs are performed with the horizontal resolution of T21 (about 5.6°×5.6°, ~333 km at equator) and vertical 49 sigma-levels (the altitude of the lowest layer is ~50 m) up to ~90 km. Also the runs with the horizontal resolution of T106 (about 1.1°×1.1°, ~67 km at equator) was performed optionally. Realistic topography, albedo, thermal inertia and roughness data for the Mars surface are introduced. Radiative effects of CO_2 gas (considering only LTE: local thermodynamic equilibrium) and dust are taken into account, and radiative effects of water ice clouds can also be included. The standard seasonal and latitudinal changes of dust opacity are defined externally, with the vertical distribution of so-called "Conrath profile" [Conrath, 1975].

The schemes of water cycle and isotopic fractionation for HDO and H_2O are implemented as described in Kuroda et al. [2012] with updates. The cloud microphysics process following Montmessin et al. [2004] is newly implemented, setting a part of airborne dust as nuclei. The number of nuclei N is defined with the function of altitude z as follows,

$$N(z) = A\frac{\tau}{\tau_{ref}} N_0 \exp(-z/H), \qquad (1)$$

where τ and τ_{ref} are the total dust opacity in the column and reference opacity (=0.1), respectively, N_0=2×10^6 m^{-3} is the reference number of nuclei, and H is the atmospheric scale height. The difference from the definition by Montmessin et al. [2004] is that we set the nuclei factor A, which we defined between 0.01 and 0.2 depending on latitude and season.

In the cloud formation scheme, the water ice cloud radius inside each grid and layer is set to be constant. The sedimentation of water ice clouds, accumulation on the surface and sublimation of water ice from the surface are implemented. The surface albedo and thermal inertia are set to be 0.35 and 800 J m^{-2} K^{-1} s$^{-1/2}$, respectively, when the water ice is accumulated for more than 5 μm without CO_2 seasonal ice cap.

About the evaporation of water vapor from surface, the turbulent flux F is defined as follows,

$$F = \beta\rho C_E |v_1|(Q_{\mathrm{sat}} - Q_1), \qquad (2)$$

where ρ is the atmospheric density, C_E is the bulk coefficient which is a function of surface roughness and atmospheric instability, v_1 is the wind velocity at the lowest layer, and Q_{sat} and Q_1 are the mass mixing ratio of water vapor at saturation and the lowest layer, respectively. In this model the effect of regolith to

absorb the water on surface is not implemented, but the evaporation efficiency β is introduced to adjust the supply of water vapor from the surface instead. The value of β is set between 0.0001 and 0.04 depending on latitude and season.

The calculations started from the 'dry' isothermal state without water vapor/ice in the atmosphere and on surface except the permanent water ice cap in the north of 80° N. The isotopic ratio of the permanent north polar water ice cap is set to 7.0 VSMOW (Vienna Standard Mean Ocean Water, [HDO]/[H_2O]= 3.1×10^{-4}).

Results:

Water vapor and ice distributions in comparison with observations

Figure 1 shows the seasonal changes of zonal-mean water vapor column density and water ice cloud opacity at ~12 μm wavelength (with a rough estimate multiplying the column density in pr.m by 10^5) in the tenth year from the isothermal state, with T21 horizontal resolution and without the radiative effects of water ice clouds. They are in overall consistent with the MGS-Thermal Emission Spectrometer (TES) observations [Smith, 2008], though drier in equinoxes. Figure 2 shows the zonal-mean ice cloud mixing ratio and the mean radius of water ice particles at L_s=90° (northern summer solstice). The simulated peak altitude of cloud abundance (~100 Pa) is approximately 10-15 km lower in comparison with MRO-Mars Climate Sounder (MCS) observation [McCleese et al., 2010] at the corresponding season (~20 Pa), and the simulated maximum cloud radius is ~12 μm. This value might be unrealistically large, but with the smaller maximum cloud radius the opacity of equatorial cloud belt is difficult to be kept high enough to fit the observations by MGS-TES.

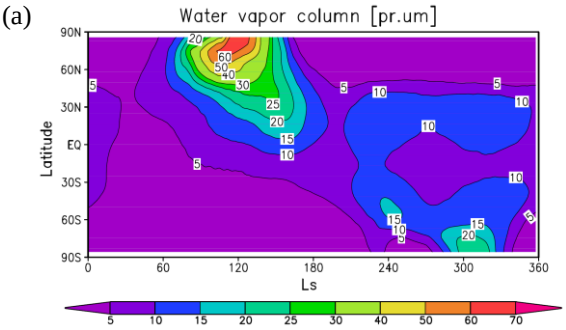

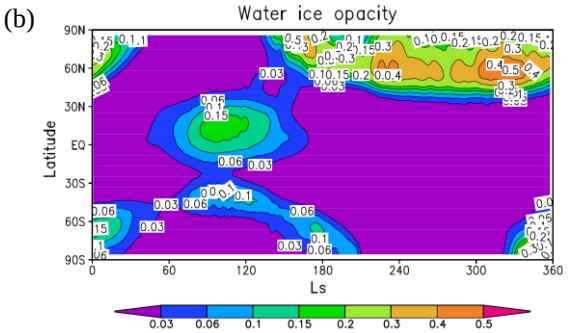

Figure 1: Simulated zonal-mean (a) water vapor column density (in pr.μm) and (b) water ice opacity at ~12 μm wavelength (rough estimate, see the text) in the tenth year from the isothermal state with T21 horizontal resolution.

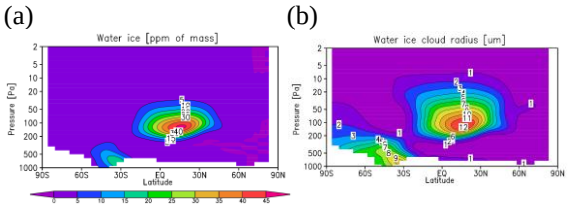

Figure 2: Simulated latitudinal-vertical cross-sections of zonal-mean (a) water ice mass mixing ratio (in ppm) and (b) radius of water ice clouds (in μm) at L_s=90° in the tenth year from the isothermal state with T21 horizontal resolution.

D/H ratio

Figure 3 shows the seasonal-latitudinal change of the HDO/H_2O ratio (in VSMOW) for the corresponding condition to Figure 1. The results are in overall consistent qualitatively with a preceding simulation by Montmessin et al. [2005]. Quantitatively the given D/H ratio of the north polar ice cap in our model is larger than Montmessin et al. [2005] (5.6 VSMOW), so the value is larger correspondingly. In comparison with the observation by Novak et al. [2011] (L_s=50°), the values in northern low- and mid-latitudes are smaller. Figure 4 shows the latitudinal-vertical cross-sections of water vapor mixing ratio and HDO/H_2O ratio in vapor at L_s=90°. The altitude of hygropause (cut-off height of water vapor) corresponds to the peak altitude of cloud abundance at equator (~100 Pa), and the vertical peak of D/H ratio in vapor appears around and slightly below the same altitude.

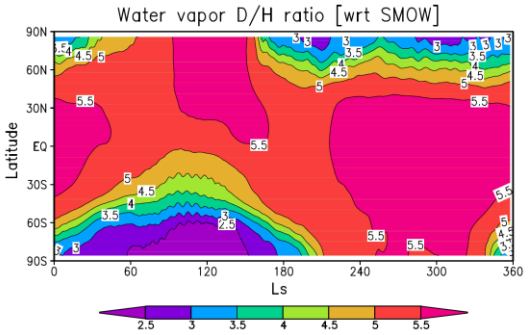

Figure 3: Simulated zonal-mean HDO/H_2O ratio in vapor (in VSMOW) corresponding to Figure 1.

(a) (b)

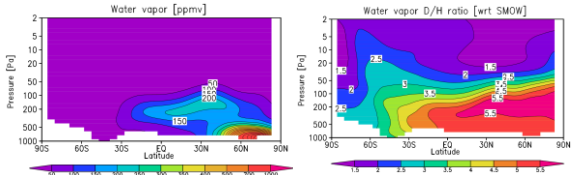

Figure 4: Simulated latitudinal-vertical cross-sections of zonal-mean (a) water vapor mixing ratio (in ppmv) and (b) HDO/H_2O ratio in vapor (in VSMOW) corresponding to Figure 2.

High-resolution simulation

Figures 5 and 6 show snapshots of water vapor column density and HDO/H_2O ratio in the high-resolution (T106) simulation at L_s~9° (northern spring), localtime of 0600 at 0° longitude. In both figures the structure of baroclinic waves with zonal wavenumbers of 1 and 2 is seen in northern mid-latitudes, as well as weaker zonal wavenumber 2 structure in southern mid-latitudes, which may transport the water vapor to polar regions. Moreover, the thermal tide may affect to strengthen the transport, as the strong flow to northeast is seen around 60° E (close to the sub-solar longitude) in northern high-latitudes. These features are more clearly seen in Figure 6, which indicates that the mapping of HDO/H_2O ratio with time sequences (for several hours or a few days) from the observations, possibly by ExoMars Trace Gas Orbiter (EMTGO) and ground-based telescopes, would work to clarify the meridional transport of water. However, it should be also noted that the longitudinal difference of D/H ratio as observed by Villanueva et al. [2015] is not reproduced in the model.

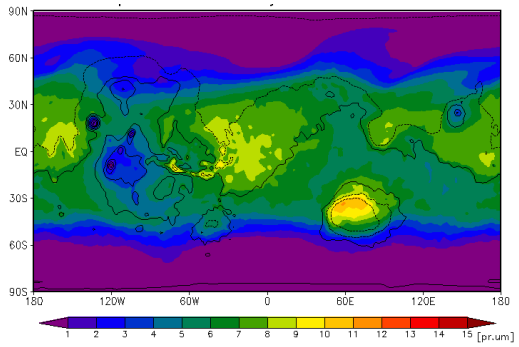

Figure 5: A snapshot of the horizontal distribution of water vapor column density in our T106 simulation, at L_s~9° at localtime of 0600 at 0° longitude.

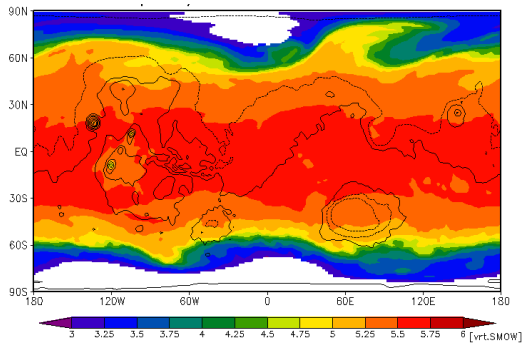

Figure 6: Same as Figure 5, except HDO/H_2O ratio in vapor column density.

With radiatively-active water ice clouds

We have also performed the calculation including the radiative effects of water ice clouds. The refractive index of water ice particles is taken from Warren [1984] and the particle size for the radiative calculation is interactive with the cloud microphysics scheme.

Figure 7 shows the simulation results at L_s=90° with the radiative effects of water ice clouds: zonal-mean temperature (in comparison with the radiatively-passive water ice clouds) and mixing ratios of water ice and vapor. The radiatively-active water ice clouds largely change the temperature fields, increasing up to ~40 K above the equator and ~20 K above the south (winter) polar region. The altitude of equatorial cloud belt and hygropause becomes 20-30 km higher (~100 Pa for radiatively-passive and ~2 Pa for radiatively-active). The opacity of equatorial cloud belt becomes ~10 times smaller than the radiatively-passive cloud simulation, and maximum cloud radius at the equatorial cloud belt becomes as small as ~2 μm (no figures).

(a) (b)

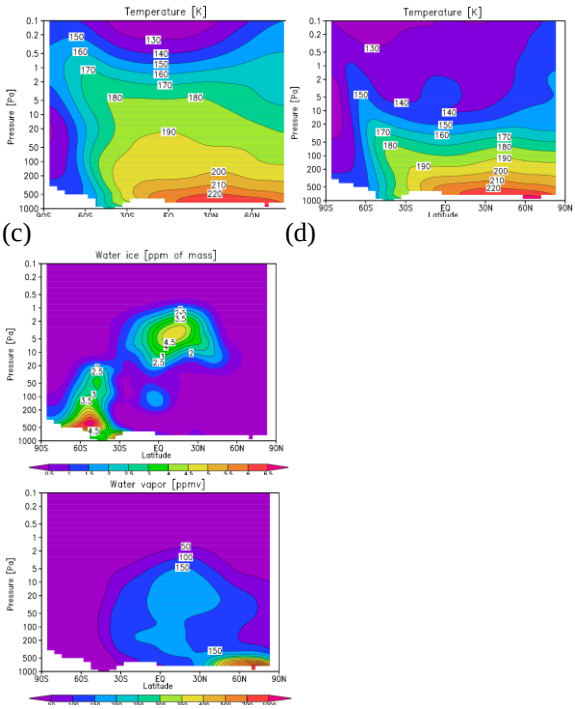

Figure 7: (a) Zonal-mean temperature at L_s=90° with radiatively-active water ice clouds. (b) Same as (a) except that the water ice clouds are radiatively-passive. (c) and (d) are same as (a) except the zonal-mean water ice mass mixing ratio and water vapor volume mixing ratio, respectively (in ppm).

Summary:

We have largely improved the water cycle scheme in the DRAMATIC MGCM from Kuroda et al. [2008, 2012], e.g. implementation of the cloud microphysics process and readjustment of surface parameter, and, therefore, the simulated seasonal-latitudinal changes of water vapor column density and water ice opacity became much closer to the MGS-TES observations than the earlier efforts, if the radiative effects of water ice clouds are not implemented. But we still have two main problems as described below for the realistic simulations: (1) We need to make the particle size of water ice in the equatorial cloud belt unrealistically large to reproduce the observed cloud opacity. (2) If the radiative effects of water ice clouds are included, the atmospheric temperature becomes unrealistically high, and also the equatorial cloud belt almost disappears. Further improvements would be needed to solve these problems, e.g. implementation of the scavenging processes as Navarro et al. [2014] did.

Despite the above problems, the DRAMATIC MGCM may be usable for the investigations of the current water environment on Mars, collaborating with the ongoing and future observations. Especially we have two main advantages: (1) HDO/H_2O isotopic fractionation and (2) horizontal high-resolution simulation are available. With this MGCM, we intend to support the MRO and EMTGO missions which observe the water in lower atmosphere, and also the MAVEN (Mars Atmosphere and Volatile Evolution) mission which observe the compositions in the upper atmosphere with future implementation of the photochemical processes and extension to the thermosphere.

References:

Conrath, B.J., 1975: Thermal Structure of the Martian Atmosphere during the Dissipation of the Dust Storm of 1971. *Icarus*, **24**, 36–46.

Haberle, R.M. et al., 2011: Radiative effects of water ice clouds on the Martian seasonal cycle. *Abstract book of 'Fourth International Workshop on the Mars Atmosphere: Modelling and Observations',* Lab. de Meteorol. Dyn., Paris, 223–225.

K-1 Model Developers, 2004: K-1 coupled GCM (MIROC) description, *K-1 Tech. Rep.*, **1**, Univ. of Tokyo, Tokyo, 1–34.

Kuroda, T. et al., 2005: Simulation of the Martian atmosphere using a CCSR/NIES AGCM, *J. Meteorol. Soc. Jpn.*, **83**, 1–19.

Kuroda, T. et al., 2008: Simulation of the water cycle on Mars in the CCSR/NIES/FRCGC MGCM. *Abstract book of 'Third International Workshop on the Mars Atmosphere: Modelling and Observations',* Lunar and Planetary Institute, Williamsburg, #9049.

Kuroda, T. et al., 2012: Modeling and observation of the water isotopic ratios on Mars: Approach to the climate changes. *Final Conference Proceeding of 'Mars Recent Climate Change Workshop'*, NASA Ames Research Center, Moffett Field, 134–137.

Kuroda, T. et al., 2013: Carbon dioxide ice clouds, snowfalls, and baroclinic waves in the northern winter polar atmosphere of Mars. *Geophys. Res. Lett.*, **40**, 1484–1488, doi:10.1002/grl.50326.

Kuroda, T. et al., 2015: A global view of gravity waves in the Martian atmosphere inferred from a high-resolution general circulation model. *Geophys. Res. Lett.*, **42**, 9213–9222, doi:10.1002/2015GL066332.

McCleese, D.J. et al., 2010: Structure and dynamics of the Martian lower and middle atmosphere as observed by the Mars Climate Sounder: Seasonal variations in zonal mean temperature, dust, and water ice aerosols. *J. Geophys. Res.*, **115**, E12016, doi:10.1029/2010JE003677.

Montmessin, F. et al., 2004: Origin and role of water ice clouds in the Martian water cycle as inferred from a general circulation model, *J. Geophys. Res.*, **109**, E10004, doi:10.1029/2004JE002284.

Montmessin, F. et al., 2005: Modeling the annual cycle of HDO in the Martian atmosphere. *J. Geophys. Res.*, **110**, E03006, doi:10.1029/2004JE002357.

Navarro, T. et al., 2014: Global climate modeling of the Martian water cycle with improved microphysics and radiatively active water ice clouds. *J. Geophys. Res. Planets*, **119**, 1479–1495, doi:10.1002/2013JE004550.

Novak, R.E. et al. 2011: Measurement of the isotopic signatures of water on Mars; Implications for studying methane. *Planet. Spa. Sci.*, **59**, 163–168, doi:10.1016/j.pss.2010.06.017.

Richardson, M.I. and R.J. Wilson, 2002: Investigation of the nature and stability of the Martian seasonal water cycle with a general circulation model. *J. Geophys. Res.*, **107**(E5), 5031, doi:10.1029/2001JE001536.

Richardson, M.I. et al., 2002: Water ice clouds in the Martian atmosphere: General circulation model experiments with a simple cloud scheme. *J. Geophys. Res.*,

107(E9), 5064, doi:10.1029/2001JE001804.

Smith, M.D., 2008: Spacecraft Observations of the Martian Atmosphere. *Annu. Rev. Earth Planet. Sci.*, **36**, 191–219, doi:10.1146/annurev.earth.36.031207.124334.

Villanueva G.L. et al., 2015: Strong water isotopic anomalies in the martian atmosphere: Probing current and ancient reservoirs. *Science,* **348**, 218–221, doi: 10.1126/science.aaa3630.

Warren, S.G., 1984: Optical constants of ice from the ultraviolet to the microwave. *Appl. Opt.,* **23**, 1206–1225.

Wilson, R.J. et al., 2008: Influence of water ice clouds on Martian tropical atmospheric temperatures. *Geophys. Res. Lett.,* **35**, L07202, doi:10.1029/2007GL032405.